PFC/JA-86-48

RELATIVISTIC NONNEUTRAL ELECTRON FLOW IN A PLANAR TRIODE

Hei W. Chan and Ronald C. Davidson
Plasma Fusion Center
Massachusetts Institute of Technology
Cambridge, MA 02139

Khanh T. Nguyen and Han S. Uhm
Naval Surface Weapons Center
Silver Spring, MD 20903

August, 1986

RELATIVISTIC NONNEUTRAL ELECTRON FLOW IN A PLANAR TRIODE

Hei W. Chan and Ronald C. Davidson
Plasma Fusion Center
Massachusetts Institute of Technology, Cambridge, Massachusetts 02139

Khanh T. Nguyen and Han S. Uhm
Naval Surface Weapons Center, Silver Spring, Maryland, 20903

ABSTRACT

The steady-state cold-fluid-Poisson equations are used to investigate the influence of space-charge effects on relativistic nonneutral electron flow in a planar triode with cathode located at $z = -L_{CA}$, anode located at $z = 0$, and a plane conductor located at $z = d$. An intense relativistic electron beam with current density $-J_0$ (generated in the diode region) is injected through the anode plane. A one-dimensional theoretical model is employed in which the spatial variations are assumed to be perpendicular to the planar conductors. Relativistic effects on the electron motion are included, but self-magnetic fields are neglected. An exact analytical expression for the relativistic current flow is obtained. The steady-state and time-averaged equilibrium properties are investigated analytically. The results are compared with approximate analytical solutions and numerical simulation results using a multiple-sheet model. Based on this investigation, it is found that the formation of a virtual cathode downstream can be suppressed by an applied electric field. The forward electron current is substantially enhanced, while the stable operating range of the steady-state triode current is reduced substantially.

I. INTRODUCTION AND SUMMARY

Several recent studies[1-3] have investigated the properties of electron beam propagation between plane conductors assuming that an intense beam of electrons, generated in the diode region, is injected into a grounded drift cavity. A one-dimensional theoretical model of the beam propagation and the concomitant collective acceleration process has been proposed by Destler, et al.[1] This model was expanded by Uhm and Sternlieb[2] to include the formation of virtual anodes downstream, and it was shown that beam propagation in an evacuated drift cavity is effectively limited by the electrostatic potential depression associated with the space charge of the unneutralized beam. However, by introducing an ion current into the system and allowing a number of virtual anodes in the downstream region, the electron current in the forward direction can be enhanced substantially. In the nonrelativistic regime, Uhm, et al.[3] have studied the properties of intense beam propagation between a grounded plane conductor and a charged plane conductor. It was found[3] that the space-charge-limited current in the downstream region can be enhanced by applying a potential at one end of the drift tube. The purpose of the present article is to extend the nonrelativistic analysis[3] for this configuration to the case of an intense relativistic electron beam propagating between plane conductors.

The triode configuration is illustrated in Fig. 1. A relativistic electron beam with current density $-J_0$, which is generated in the diode region, is injected through the anode plane in the z-direction. The present one-dimensional model is based on the cold-fluid-Poisson equations in which the spatial variations are assumed to be perpendicular to the plane conductors, and self-magnetic fields are neglected.

The basic assumptions and theoretical model are described in Sec. II, and the steady-state equilibrium properties of an electron beam propagating between plane conductors are investigated. An exact analytical solution for the relativistic current flow between two plane conductors is obtained [Eq.(22)] in terms of the electron injection energy γmc^2 and other system parameters. For specified electron energy, we find that there exists a critical injection current density J_c, below which steady-state solutions exist. This critical current density can be increased substantially by an applied electric field.

Allowing for an electron return current, the time-averaged solutions for $J_0 \geq J_c$ are investigated in Sec. III.A, where it is shown that the forward electron current is enhanced by an applied electric field. In Sec. III.B, the time-averaged solutions for $J_0 >> J_c$ are modified substantially by the large return current injected back into the diode region. An approximate solution for the steady-state current flow is obtained in Sec. III.C [Eq.(40)], and the results are found to be in excellent agreement with the exact analytical solution [Eq.(22)].

Finally, Sec. IV presents a one-dimensional simulation of the time-evolution of the relativistic electron flow between two plane conductors. The simulation results agrees well with the analytical predictions in Sec. II and III.

II. THEORETICAL MODEL AND STEADY-STATE EQUILIBRIUM

In the present analysis, we make use of the cold-fluid-Poisson equations to investigate the properties of relativistic nonneutral electron flow in a planar triode. The triode configuration is illustrated in Fig. 1. The cathode (with electrostatic potential $\phi = -V_0$) is located at $z = -L_{CA}$; the anode is located at $z = 0$ (with $\phi = 0$); and a charged conductor is located at $z = d$ (with $\phi = V$). A relativistic nonneutral electron beam with uniform current density $-J_0$, generated in the cathode-anode region, is injected through the anode plane in the z-direction. It is assumed that the electrons traverse the anode plane without collisions, and that they are absorbed completely by the right-most conductor at $z = d$. Since the conductors are assumed to be infinite planes, the influence of self-magnetic fields is neglected in the present analysis. In this context, the treatment reduces to an analysis of the one-dimensional cold-fluid-Poisson equations.

It is convenient to divide the planar triode into the diode region (cathode-anode region) and the downstream region such that each region can be treated separately, provided the proper boundary conditions are satisfied at the interface $z = 0$. For future reference, the magnitude of the current density J_{CA} for relativistic space-charge-limited flow in a planar diode has been shown by Jory and Trivelpiece[4] to be given by[5]

$$J_{CA} = \frac{mc^3}{8\pi e L_{CA}^2}\left[\int_1^{\gamma_0}\frac{d\gamma}{(\gamma^2-1)^{\frac{1}{4}}}\right]^2 \tag{1}$$

$$= \frac{mc^3}{8\pi e L_{CA}^2}\left[F\left(\delta_0,\ 2^{-\frac{1}{2}}\right) - 2E\left(\delta_0,\ 2^{-\frac{1}{2}}\right) + \frac{2\gamma_0(\gamma_0^2-1)^{\frac{1}{4}}}{1+(\gamma_0^2-1)^{\frac{1}{2}}}\right]^2 ,$$

where δ_0 and γ_0 are defined by

$$\delta_0 = \cos^{-1}\left[\frac{1 - (\gamma_0^2 - 1)^{\frac{1}{2}}}{1 + (\gamma_0^2 - 1)^{\frac{1}{2}}}\right] ,$$

$$\gamma_0 = 1 + \frac{eV_0}{mc^2} .$$

Here, -e is the electron charge, m is the electron rest mass, c is the speed of light in vacuo, and L_{CA} is the cathode-anode spacing (Fig. 1). Moreover, $F(\delta,k)$ and $E(\delta,k)$ are elliptic integrals of the first and second kind, respectively, defined by

$$F(\xi,k) = \int_0^{\sin\xi} dx \left[(1 - x^2)(1 - k^2x^2)\right]^{-\frac{1}{2}} ,$$

$$E(\xi,k) = \int_0^{\sin\xi} dx\,(1 - k^2x^2)^{\frac{1}{2}}\,(1 - x^2)^{-\frac{1}{2}} .$$

As illustrated in Fig. 1, we assume that the diode current $-J_0$ is injected through the anode plane and propagates in the downstream region defined by $0 \leq z \leq d$. The amount of beam current that can propagate in this region is limited by the electrostatic potential depression associated with the beam space charge. The space-charge-limited equilibrium current can be determined from Poisson's equation, the equation of continuity, and the conservation of energy, under steady-state conditions.

The steady-state Poisson equation in the region between the two plane conductors ($0 \leq z \leq d$) is given by

$$\frac{\partial^2\phi(z)}{\partial z^2} = -4\pi\rho(z) , \qquad (2)$$

where $\phi(z)$ is the electrostatic potential, and the charge density $\rho(z)$ is defined by

$$\rho(z) = \frac{J(z)}{\beta(z)c} \ . \tag{3}$$

Here, $J(z)$ is the current density, and $\beta(z)$ is the ratio of the electron flow velocity $V_z(z)$ to the speed of light. Equation (2) is to be solved subject to the boundary conditions (Fig. 1)

$$\begin{aligned} \phi(z = 0) &= 0 \ , \\ \phi(z = d) &= V \ . \end{aligned} \tag{4}$$

The electrostatic potential profile $\phi(z)$ in the region between the two plane conductors is illustrated schematically in Fig. 2. Moreover, the relativistic flow velocity $\beta(z)c$ and the potential $\phi(z)$ are related by the conservation of energy,

$$-e\phi(z) + \left[\frac{1}{\sqrt{1 - \beta(z)^2}} - 1\right] mc^2 = eV_0 \ , \tag{5}$$

where $-V_0$ is the cathode voltage. For notational convenience in the subsequent analysis, the relativistic mass factors $\gamma(z)$ and γ_0 are introduced, where

$$\gamma(z) = \left[1 - \beta(z)^2\right]^{-\frac{1}{2}} = 1 + \frac{e[V_0 + \phi(z)]}{mc^2} \ , \tag{6}$$

$$\gamma_0 = 1 + \frac{eV_0}{mc^2} \ . \tag{7}$$

Steady-state equilibrium solutions exist for current density $-J_0$ below the space-charge limit. In this case, charge conservation implies $\nabla \cdot \underset{\sim}{J} = 0$, which gives $J(z) = -J_0 = \text{const}$. Substituting Eqs.(3) and (6) into Eq.(2) then gives

$$\frac{\partial^2 \gamma}{\partial z^2} = \left(\frac{4\pi e J_0}{mc^3}\right) \frac{\gamma}{(\gamma^2 - 1)^{\frac{1}{2}}} \quad . \tag{8}$$

As illustrated in Fig. 2, the boundary conditions in Eq.(8) are

$$\left(\frac{\partial \gamma}{\partial z}\right)_{z = d_m} = 0 = \left(\frac{\partial \phi}{\partial z}\right)_{z = d_m} \quad , \tag{9}$$

where d_m represents the axial location of the minimum potential ϕ_m, i.e., $\phi(z = d_m) \equiv \phi_m$. Earlier derivations[4] have not taken into account this important boundary condition. We make the following change of variables in Eq.(8)

$$y = \frac{\partial \gamma}{\partial z} \quad . \tag{10}$$

Making use of

$$y \frac{\partial y}{\partial \gamma} = \frac{\partial^2 \gamma}{\partial z^2} \quad , \tag{11}$$

Eq.(8) can be expressed in the equivalent form

$$y \frac{\partial y}{\partial \gamma} = \frac{4\pi e J_0}{mc^3} \frac{\gamma}{(\gamma^2 - 1)^{\frac{1}{2}}} \quad . \tag{12}$$

Equation (12) can be integrated over the region with boundary conditions in Eq.(9) to give

$$y^2 = \frac{8\pi e J_0}{mc^3} \left[(\gamma^2 - 1)^{\frac{1}{2}} - (\gamma_m^2 - 1)^{\frac{1}{2}}\right] \quad . \tag{13}$$

Taking the square root of Eq.(13) and making use of Eq.(10), it follows that Eq.(13) can be integrated over the regions $z < d_m$ and $z > d_m$ using the respective boundary conditions in Eq.(4). This gives

$$-\left(\frac{mc^3}{8\pi eJ_0}\right)^{\frac{1}{2}}\int_{\gamma_m}^{\gamma_0}\frac{d\gamma}{[(\gamma^2-1)^{\frac{1}{2}}-(\gamma_m^2-1)^{\frac{1}{2}}]^{\frac{1}{2}}}=\int_{d_m}^{0}dz=-d_m,\quad z<d_m\ , \tag{14}$$

and

$$\left(\frac{mc^3}{8\pi eJ_0}\right)^{\frac{1}{2}}\int_{\gamma_m}^{\gamma_d}\frac{d\gamma}{[(\gamma^2-1)^{\frac{1}{2}}-(\gamma_m^2-1)^{\frac{1}{2}}]^{\frac{1}{2}}}=\int_{d_m}^{d}dz=d-d_m,\quad z>d_m\ , \tag{15}$$

where γ_m and γ_d are the relativistic mass factors at $z = d_m$ and $z = d$, respectively. Combining Eqs.(14) and (15) and solving for J_0, we obtain

$$J_0(\gamma_0,\gamma_m,\gamma_d)=\frac{mc^3}{8\pi ed^2}\left[\int_{\gamma_m}^{\gamma_0}\frac{d\gamma}{[(\gamma^2-1)^{\frac{1}{2}}-(\gamma_m^2-1)^{\frac{1}{2}}]^{\frac{1}{2}}}+\int_{\gamma_m}^{\gamma_d}\frac{d\gamma}{[(\gamma^2-1)^{\frac{1}{2}}-(\gamma_m^2-1)^{\frac{1}{2}}]^{\frac{1}{2}}}\right]^2. \tag{16}$$

Equation (16) constitutes a formal expression for the characteristic current density $J_0(\gamma_0,\gamma_m,\gamma_d)$ propagating between the two plane conductors at $z = 0$ and $z = d$. Here, $\gamma_m = \gamma(z = d_m)$ and $\gamma_d = \gamma(z = d)$ are defined by [see Fig. 1 and Eq.(6)]

$$\gamma_m = 1 + e(V_0 + \phi_m)/mc^2\ ,$$

$$\gamma_d = 1 + e(V_0 + V)/mc^2\ ,$$

where $\phi_m = \phi(z = d_m)$.

The integrals in Eq.(16) can be evaluated exactly by making the change of variable[4]

$$w = (\gamma^2 - 1)^{\frac{1}{2}}\ . \tag{17}$$

Then the integral I, defined by

$$I = \int_{\gamma_m}^{\gamma(\phi)} \frac{d\gamma}{[(\gamma^2 - 1)^{\frac{1}{2}} - (\gamma_m^2 - 1)^{\frac{1}{2}}]^{\frac{1}{2}}} \quad , \tag{18}$$

can be transformed to

$$I = \int_{w_m}^{w(\gamma)} \frac{wdw}{[(w - w_m)(w^2 + 1)]^{\frac{1}{2}}} \quad , \tag{19}$$

where $w_m = (\gamma_m^2 - 1)^{\frac{1}{2}}$. Equation (19) has the form of a standard elliptic integral[6] which can be expressed as

$$I = \left[\frac{(a+b)^2}{g} \frac{(1+\cos\varphi)}{\sin\varphi} (1 - k^2\sin^2\varphi)^{\frac{1}{2}} - \frac{(a+b)b}{g} F(\varphi,k) + \frac{(a+b)^2}{g} E(\varphi,k) \right]_{\varphi_m}^{\varphi(w)} \tag{20}$$

Here, $F(\varphi,k)$ and $E(\varphi,k)$ are incomplete elliptic integrals of the first and second kinds, respectively, and the quantities a, b, g, k and $\varphi(w)$ are defined by

$$g = 2\gamma_m^{3/2} \quad ,$$

$$a = \frac{1}{b} = \left[\frac{\gamma_m - (\gamma_m^2 - 1)^{\frac{1}{2}}}{\gamma_m + (\gamma_m^2 - 1)^{\frac{1}{2}}} \right]^{\frac{1}{2}} \quad , \tag{21}$$

$$k = \left[\frac{\gamma_m - (\gamma_m^2 - 1)^{\frac{1}{2}}}{2\gamma_m} \right]^{\frac{1}{2}} \quad ,$$

$$\varphi(w) = \cos^{-1}\left(\frac{w - b}{w + a} \right) \quad .$$

Making use of Eq.(20), the characteristic current density in Eq.(16) can be expressed as

$$J_0(\varphi_0,\varphi_m,\varphi_d) = \frac{mc^3}{8\pi ed^2}\,[H(\varphi_0,\varphi_m) + H(\varphi_d,\varphi_m)]^2 \quad , \tag{22}$$

where the function $H(\varphi_1,\varphi_2)$ is defined by

$$H(\varphi_1,\varphi_2) = \frac{(a+b)^2}{g}\left[\frac{(1+\cos\varphi_1)}{\sin\varphi_1}\,(1 - k^2\sin^2\varphi_1)^{\frac{1}{2}} - \frac{(1+\cos\varphi_2)}{\sin\varphi_2}\,(1 - k^2\sin^2\varphi_2)^{\frac{1}{2}}\right]$$

$$- \frac{(a+b)b}{g}\,[F(\varphi_1,k) - F(\varphi_2,k)] \tag{23}$$

$$+ \frac{(a+b)^2}{g}\,[E(\varphi_1,k) - E(\varphi_2,k)] \ .$$

It is instructive to consider the special case where $\phi_m = -V_0$ and $V = 0$, corresponding to space-charge-limited flow. Equation (22) then reduces to

$$J_0(\gamma_m = 1,\ \gamma_d = \gamma_0) \equiv J_{sc}$$

$$= \frac{mc^3}{8\pi e(d/2)^2}\left[\int_1^{\gamma_0} \frac{d\gamma}{(\gamma^2 - 1)^{\frac{1}{2}}}\right]^2 \tag{24}$$

$$= \frac{mc^3}{8\pi e(d/2)^2}\,[H(\varphi_0,\pi)]^2 \ ,$$

which is identical to the time-independent relativistic Child's law obtained by Jory and Trivelpiece[4] for a planar diode with an effective cathode-anode spacing L_{CA} equal to d/2 [see Eq.(1)]. Making use of the definition in Eq.(24),

the characteristic current density in Eq.(22) can generally be expressed as

$$\frac{J_0}{J_{sc}} = \left[\frac{H(\varphi_0,\varphi_m) + H(\varphi_d,\varphi_m)}{2H(\varphi_0,\pi)} \right]^2 . \tag{25}$$

To illustrate the influence of the injection current density on the space-charge field, the characteristic curves obtained from Eq.(25) are shown in Fig. 3, where the absolute value of the normalized mimimum potential $|\phi_m|/V_0$ is plotted versus J_0/J_{sc} for several values of V/V_0. Several points are noteworthy in Fig. 3. First, for a specified value of V/V_0, steady-state solutions for $|\phi_m|/V_0$ exist only when J_0 is smaller than a critical value $J_c(\gamma_0)$ corresponding to the maximum allowable value of J_0. Defining the critical potential by $\phi_c(\gamma_0) \equiv \phi_m(J_0 = J_c)$, we obtain

$$J_c = \frac{mc^3}{8\pi ed^2} [H(\varphi_0,\varphi_c) + H(\varphi_d,\varphi_c)]^2 , \tag{26}$$

where $H(\varphi_1,\varphi_2)$ is defined in Eq.(23), and φ_c and γ_c are defined by

$$\varphi_c = \cos^{-1}\left[\frac{(\gamma_c^2 - 1)^{\frac{1}{2}} - b}{(\gamma_c^2 - 1)^{\frac{1}{2}} + a} \right] ,$$

$$\gamma_c = 1 + \frac{e(V_0 + \phi_c)}{mc^2} .$$

As an example, we take $\gamma_0 = 5$ and $V = 0$ [see Fig. 3(b)]. Then the critical value of current density is $J_c = 1.53\ J_{sc}$, and the critical potential is $\phi_c = -0.89\ V_0$. Second, for the range $0 < J_0 < J_{sc}$, it is evident that

$\phi_m(J_0)$ is a single-valued function of J_0. Moreover, for the range $J_{sc} < J_0 < J_c$, there are two different values of $|\phi_m|$ for a specified value of J_0. However, only the smaller of these two values is a stable and physically attainable solution. It is evident that the condition $\phi_m = -V_0$ and $J_0 = J_{sc}$ can never be achieved under steady-state conditions. Third, we find that the critical potential ϕ_c approaches zero as the parameter V/V_0 increases. Moreover, relativistic effects shift the critical potential ϕ_c toward higher value of ϕ_m. Finally, for sufficiently large values of V/V_0, it is evident from both Figs. 3(a) and 3(b) that the characteristic current remains fairly flat over a wide range of $|\phi_m|/V_0$.

For $\gamma_0 > 1$ and $V = 0$, it should be pointed out that our results are in good qualitative agreement with those obtained by Uhm and Sternlieb[2]. Moreover, the results for $\gamma_0 = 1.001$ agree well with the nonrelativistic solutions obtained by Uhm, et al.[3] [See Fig. 3(a).]

III. APPROXIMATE SOLUTIONS

A. Time-Averaged Solution with Return Current

When the injection current density J_0 exceeds the critical current density J_c, excess charge will accumulate in the region of the potential minimum until ϕ_m achieves the value $\phi_m = -V_0$, at which time a portion of the injected beam will be reflected back toward the anode at $z = 0$. The process leading to the state $\phi_m = -V_0$ is nonadiabatic, and $|\phi_m|$ can be temporarily larger than V_0, eventually oscillating about the value $\phi_m = -V_0$. We can average over this nonlinear, time-dependent oscillatory behavior by making the time-averaged approximation[1,2] that a virtual cathode with $\phi_m = -V_0$ is formed at $z = d_m$. Allowing for an electron return current, it is evident that the electron charge density can be expressed as

$$\rho(z) = \begin{cases} \dfrac{-pJ_0}{\beta(z)c} , & z > d_m , \\ \dfrac{(p-2)J_0}{\beta(z)c} , & z < d_m . \end{cases} \tag{27}$$

Here, p represents the ratio of the electron current density J_f in the forward direction to the injection current density J_0. It is further assumed that the counter-streaming electrons are non-collisional, and that the return current injected back into the diode region is negligibly small and does not significantly modify the injection current J_0. Substituting Eq.(27) into Eq.(2), and making use of Eq.(6) and $(\partial\gamma/\partial z)_{z=d_m} = 0$ in Eq.(9), we obtain

$$\left(\frac{\partial\gamma}{\partial z}\right)^2 = \left(\frac{8\pi e J_0}{mc^3}\right) \times \begin{cases} (2-p)(\gamma^2-1)^{\frac{1}{2}} , & 0 < z < d_m , \\ p(\gamma^2-1)^{\frac{1}{2}} , & d_m < z < d . \end{cases} \tag{28}$$

Integrating Eq.(28) over γ and making use of the appropriate changes of variables in Eqs.(10) and (17), we obtain

$$J_0 = \frac{mc^3}{8\pi ed^2}\left[\int_1^{\gamma_0} \frac{d\gamma}{[(2-p)(\gamma^2-1)^{\frac{1}{2}}]^{\frac{1}{2}}} + \int_1^{\gamma_d} \frac{d\gamma}{[p(\gamma^2-1)^{\frac{1}{2}}]^{\frac{1}{2}}}\right]^2$$
$$= \frac{mc^3}{8\pi ed^2}\left[\frac{H(\varphi_0,\varphi_m)}{(2-p)^{\frac{1}{2}}} + \frac{H(\varphi_d,\varphi_m)}{p^{\frac{1}{2}}}\right]^2 , \tag{29}$$

where $H(\varphi_1,\varphi_2)$ is defined in Eq.(23). In order to illustrate the influence of the applied voltage V at z = d, we plot in Fig. 4 the normalized characteristic current J_0/J_{sc} versus the parameter p for several values of V/V_0. For a given value of injection current density J_0, it is evident that the fraction of the injection current that is transmitted is significantly enhanced by increasing the applied voltage V.

It is perhaps more insightful to eliminate J_0 in favor of the cathode-anode spacing L_{CA}. Because the injection current density J_0 is equal to the space-charge-limited current density in the cathode-anode region, the current ratio J_0/J_{sc} can be expressed as

$$\frac{J_0}{J_{sc}} = \frac{J_{CA}}{J_{sc}} = \left(\frac{d}{2L_{CA}}\right)^2 , \tag{30}$$

where use has been made of Eqs.(1) and (24). It is evident from Fig. 4 [replacing J_0/J_{sc} by $(d/2L_{CA})^2$] that as d (the separation between the two plane conductors) is increased with respect to the cathode-anode spacing L_{CA}, a smaller fraction of the injection current reaches the conductor at z = d. Moreover, in the limit where $J_0 = J_{CA} \to \infty$ and $p \to 0$, the forward current density J_f defined by

$$|J_f| = pJ_0$$
$$= \frac{mc^3}{8\pi ed^2}\left[\left(\frac{p}{2-p}\right)^{\frac{1}{2}} H(\varphi_0,\varphi_m) + H(\varphi_d,\varphi_m)\right]^2 \tag{31}$$

approaches the limit

$$|J_f| \to \left(\frac{mc^3}{8\pi ed^2}\right)[H(\varphi_d,\varphi_m)]^2 .$$

B. Time-Averaged Solution with Back Injection

In the case when the injection current density J_0 is much larger than the critical current density J_c, the amount of return current injected back into the diode region is substantial and the injection current J_0 must now include the dependence on p. We denote the new injection current density by J_0'. Making use of the same time-averaged approximation as in Sec. III.A, we include the space-charge contribution from the electron return current. The charge density in the diode region can then be expressed as

$$\rho(z) = \frac{(p-2)J_0'}{\beta(z)c} . \tag{32}$$

Substituting Eq.(32) into Poisson's equation (2), it is evident that $(p-2)J_0' = J_{CA}$ is required in order for Child's law to be satisfied. Here, J_{CA} is the space-charge-limited current density in the diode region [Eq.(1)]. Therefore, the net current density injected into the downstream region is given by

$$J_0' = \frac{J_{CA}}{(2-p)} . \tag{33}$$

Replacing J_0 in Eq.(29) by J_0', the quantity p can be expressed as

$$p = 2\left\{[H(\varphi_d,\varphi_m)]^{-2}\left[\left(\frac{J_{CA}}{mc^3/8\pi ed^2}\right)^{\frac{1}{2}} - H(\varphi_0,\varphi_m)\right]^2 + 1\right\}^{-1}$$

$$= 2\left\{\left[\left(\frac{d}{L_{CA}} - 1\right)\frac{H(\varphi_0,\varphi_m)}{H(\varphi_d,\varphi_m)}\right]^2 + 1\right\}^{-1} , \tag{34}$$

where $H(\varphi_1,\varphi_2)$ is defined in Eq.(23).

Moreover, the equation for the characteristic current becomes

$$\frac{J_0'}{J_{sc}} = \frac{J_{CA}}{(2-p)J_{sc}} = \frac{1}{(2-p)}\left(\frac{d}{2L_{CA}}\right)^2 , \tag{35}$$

where p is as defined in Eq.(34). For the special case where V = 0, it is readily shown that Eq.(34) reduces to

$$p = 2\left\{\left(\frac{d}{L_{CA}} - 1\right)^2 + 1\right\}^{-1} . \tag{36}$$

Furthermore, for V = 0, it is evident that $d/2 \geq L_{CA}$ and $0 \leq p \leq 1$ are satisfied.

C. Approximate Steady-State Solutions

In this section, the expression for the steady-state current flow in Eq.(16) is simplified in the nonrelativistic limit, $\gamma \to 1$, and in the ultra-relativistic limit, $\gamma >> 1$. An approximate analytical expression, applicable over a wide energy range, is obtained.

The solution for a nonrelativistic planar triode has been obtained previously[3] and the results are summarized here. Replacing the kinetic energy term $[\gamma(z) - 1]mc^2$ in Eq.(5) by $(m/2)v(z)^2$ in the limit $\gamma \to 1$, the Poisson

equation (2) can be solved to give the nonrelativistic expression for the current density in the downstream region, i.e.,

$$J_N = \frac{cV_0}{9\pi d^2}\left(\frac{2eV_0}{mc^2}\right)^{\frac{1}{2}}\left[(1-\xi)^{\frac{1}{2}}(1+2\xi)+(\eta-\xi)^{\frac{1}{2}}(\eta+2\xi)\right]^2 \quad . \tag{37}$$

Here, the parameters η and ξ are defined by

$$\xi = \left(1 - \frac{|\phi_m|}{V_0}\right)^{\frac{1}{2}} \quad ,$$

$$\eta = \left(1 + \frac{V}{V_0}\right)^{\frac{1}{2}} \quad .$$

For the special case where $|\phi_m| = V_0$ and $V = 0$, the expression for current density in Eq.(37) reduces to

$$J_{sc} = \frac{1}{9\pi}\left(\frac{2e}{m}\right)^{\frac{1}{2}}\frac{V_0^{3/2}}{(d/2)^2} \quad , \tag{38}$$

which is identical to the classical, time-independent, nonrelativistic Child's Law[7,8] for a planar diode with an effective cathode-anode spacing L_{CA} equal to d/2.

In the limit where $\gamma >> 1$, the expression for current density in Eq.(16) can be simplified easily to give the ultrarelativistic result

$$J_U = \frac{cV_0}{2\pi d^2}\left[(1-\xi)^{\frac{1}{2}}(1+\xi)^{\frac{1}{2}}+(\eta-\xi)^{\frac{1}{2}}(\eta+\xi)^{\frac{1}{2}}\right]^2 \quad . \tag{39}$$

A simple analytical approximation to the exact steady-state current density [Eq.(22)] in the downstream region can be obtained by taking the

weighted sum of the two limiting expressions in Eqs.(37) and (39). The plausible weighting factors for the nonrelativistic and the ultra-relativistic terms are $(1/\gamma_0)^{3/2}$ and $[(\gamma_0 - 1)/\gamma_0]^{3/2}$, respectively, where $\gamma_0 = 1 + eV_0/mc^2$. The resulting approximate expression for the steady-state current density is given by

$$J_A = \left(\frac{1}{\gamma_0}\right)^{3/2} J_N + \left(\frac{\gamma_0 - 1}{\gamma_0}\right)^{3/2} J_U \quad . \tag{40}$$

In the limits where $\gamma_0 \to 1$, or $\gamma_0 \to \infty$, Eq.(40) reduces to the expressions for the limiting current density in Eqs.(37) and (39), respectively. In Fig. 5, for typical values of ϕ_m and V, it is shown that the approximate result in Eq.(40) is in excellent agreement with the exact solution [Eq.(22)] over a wide range of eV_0/mc^2.

IV. NUMERICAL SIMULATIONS

The space-charge effects of an intense relativistic electron beam with $J_0 > J_c$ are investigated in this section, including the influence of a return current. As in Sec. II, a one-dimensional model is used, and the effects of self-magnetic fields are neglected. The electron beam is injected through the anode into the region between the two plane conductors shown in Fig. 1. The return current injected back into the diode region is neglected. The subsequent temporal and spatial evolution of the beam are studied by computer simulation with time measured in units of the free-electron transit time τ between the two plane conductors, i.e.,

$$\tau = \frac{d}{\beta_0 c} \quad . \tag{40}$$

A one-dimensional simulation code based on the multiple-sheet model[9] has been developed to investigate the properties of an intense relativistic electron beam propagating between two plane conductors. The approach used to investigate this nonlinear, time-dependent problem is to represent the electron beam as a large number of charged sheets or super-particles. These negatively-charged, plane sheets are injected into the system at equal time intervals. The Poisson equation is solved self-consistently at each time interval to determine the electric force exerted on each charged sheet. Approximately 500 sheets are admitted into the system during each simulation.

To illustrate the influence of an axial energy spread on the oscillatory behavior observed for beams with $J_0 > J_c$, we assume in the present one-dimensional model that the transverse energy spread is negligible and that the thermal velocity distribution in the z-direction can be approximated by[10]

$$v = v_0(1 - W\log R)^{\frac{1}{2}} , \tag{41}$$

where $W = kT_c/eV_0$ and $v_0 = \beta_0 c$. Here, T_c is the (small) cathode temperature, and R is a random number in the interval $0 \leq R \leq 1$.

Typical simulation results are illustrated in Figs. 6-8. Shown in Fig. 6 are temporal plots of the normalized minimum potential $|\phi_m|/V_0$ for the choice of system parameters $\gamma_0 = 5$, $W = 0$, $J_0 = 2J_{sc} = 1.3\ J_c$, and $V = 0$ [Fig. 6(a)] and $V = V_0$ [Fig. 6(b)]. It is evident from Fig. 6 that a sufficiently strong applied electric field effectively suppresses the formation of a virtual cathode and hence permits the full current to be transmitted as predicted in Sec. III.A.

Figure 7 shows plots of $|\phi_m|/V_0$ versus t/τ for the choice of parameters $\gamma_0 = 5$, $J_0 = 1.67\ J_{sc} = 1.1\ J_c$, $V = 0$, and $W = 0$ [Fig. 7(a)] and $W = 0.005$ [Fig. 7(b)]. It is evident that the oscillation amplitude is significantly reduced by a small axial energy spread. Moreover, the average magnitude of the minimum potential $|\phi_m|$ is increased by increasing the effective energy spread W.

Figure 8 shows plots of $|\phi_m|/V_0$ versus t/τ for the choice of parameters $\gamma_0 = 5$, $W = 0$, $V = 10\ V_0$, and $J_0 = 1.05\ J_c$ [Fig. 8(a)] and $J_0 = 0.95\ J_c$ [Fig. 8(b)]. For sufficiently high applied electric field, it is found that a small perturbation about J_c can take the system out of steady-state operation into an oscillatory mode, and vice-versa.

In agreement with earlier numerical results[1,2] for $J_0 \geq J_c$, the minimum potential position d_m is found to exhibit a similar oscillatory behavior to that of the minimum potential ϕ_m. In the absence of an applied electric field, the minimum potential position d_m remains at d/2 until ϕ_m achieves the value $-V_0$, at which time d_m shifts closer to the anode at $z = 0$ and oscillates

about this new location with a frequency identical to that of the minimum potential ϕ_m. In the presence of an applied electric field, the location of virtual cathode formation and its position of oscillation is shifted closer to the cathode.

V. CONCLUSIONS

In this paper, we have investigated the properties of relativistic nonneutral electron flow between plane conductors. The steady-state and time-averaged equilibrium properties of the electron beam were calculated within the framework of the cold-fluid-Poisson equations. An exact analytical solution for the relativistic characteristic current density J_0 was obtained in Sec. II. The time-averaged solution for the case where the electron injection current exceeds the critical current was investigated in Sec. III.A, and the influence of a return current injected back into the diode region was examined in Sec. III.B. An approximate solution for the relativistic characteristic current was derived in Sec. III.C, which gives an excellent estimate of the characteristic current over a wide parameter range. Finally, computer simulation results were presented in Sec. IV, which agree well with the analytical predictions in Sec. II. Based on this investigation, it is found that the formation of a virtual cathode downstream can be suppressed by an applied electric field. The forward electron current is substantially enhanced, while the stable operational range of the steady-state triode current is reduced substantially.

ACKNOWLEDGMENTS

This work was supported by the Independent Research Fund at the Naval Surface Weapons Center and in part by the Office of Naval Research.

VI. REFERENCES

1. W.W. Destler, H.S. Uhm, H. Kim and M.P. Reiser, J. Appl. Phys. 50, 3015 (1979).
2. H.S. Uhm and A. Sternlieb, Phys. Fluids 23, 1400 (1980).
3. H.S. Uhm, W. Namkung and K.T. Nguyen, Naval Surface Weapons Center Report NSWC MP 85-240 (1985), submitted for publication.
4. H.R. Jory and A.W. Trivelpiece, J. Appl. Phys. 40, 3924 (1969).
5. R.B. Miller, An Introduction to the Physics of Intense Charged Particle Beams (Plenum, New York, 1982).
6. W. Grobner and N. Hofreiter, Integraltafel-Unbestimmte Integrale (Springer-Verlag, Wien and Innsbruck, 1949).
7. C.D. Child, Phys. Rev. 32, 492 (1911).
8. I. Langmuir, Phys. Rev. 2, 450 (1913).
9. C.K. Birdsall and W.B. Bridges, Electron Dynamics of Diode Regions (Academic, New York, 1966).
10. P.K. Tien and J. Moshman, J. Appl. Phys. 27, 1067 (1956).

FIGURE CAPTIONS

Fig. 1. Schematic of planar triode geometry.

Fig. 2. Schematic plot of the electrostatic potential profile $\phi(z)$ in the downstream region [Eq.(8)].

Fig. 3. Plots of the characteristic curves for J_0/J_{sc} versus $|\phi_m|/V_0$ obtained from Eq.(25) for (a) $\gamma_0 = 1.001$ and (b) $\gamma_0 = 5$, and several values of V/V_0.

Fig. 4. Plots of the characteristic curves for J_0/J_{sc} versus p obtained from Eq.(29) for (a) $\gamma_0 = 1.001$ and (b) $\gamma_0 = 5$, and several values of V/V_0.

Fig. 5. Plots of the normalized current density $\pi d^2 J_0/cV_0$ versus eV_0/mc^2 obtained from the exact [Eq.(22)] and approximate [Eq.(40)] solutions for the choice of system parameters $|\phi_m| = 0.8\ V_0$ and $V = 5\ V_0$. The nonrelativistic and ultrarelativistic curves in Fig. 5 correspond to the limiting expressions in Eqs.(37) and (39), respectively.

Fig. 6. Computer simulation plots of the normalized minimum potential $|\phi_m|/V_0$ versus t/τ for $\gamma_0 = 5$, $J_0 = 2\ J_{sc} = 1.3\ J_C$, $W = 0$, and (a) $V = 0$ and (b) $V = V_0$. Figure 6(b) illustrates the suppression of virtual cathode formation by an applied electric field.

Fig. 7. Computer simulation plots of $|\phi_m|/V_0$ versus t/τ for $\gamma_0 = 5$, $J_0 = 1.67\ J_{sc} = 1.1\ J_C$, $V = 0$, and (a) $W = 0$ and (b) $W = 0.005$. Figure 7(b) illustrates the influence of an axial energy spread on suppressing oscillatory behavior.

Fig. 8. Computer simulation plots of $|\phi_m|/V_0$ versus t/τ for $\gamma_0 = 5$, $W = 0$, $V = 10\ V_0$, and (a) $J_0 = 1.05\ J_C$ and (b) $J_0 = 0.95\ J_C$.

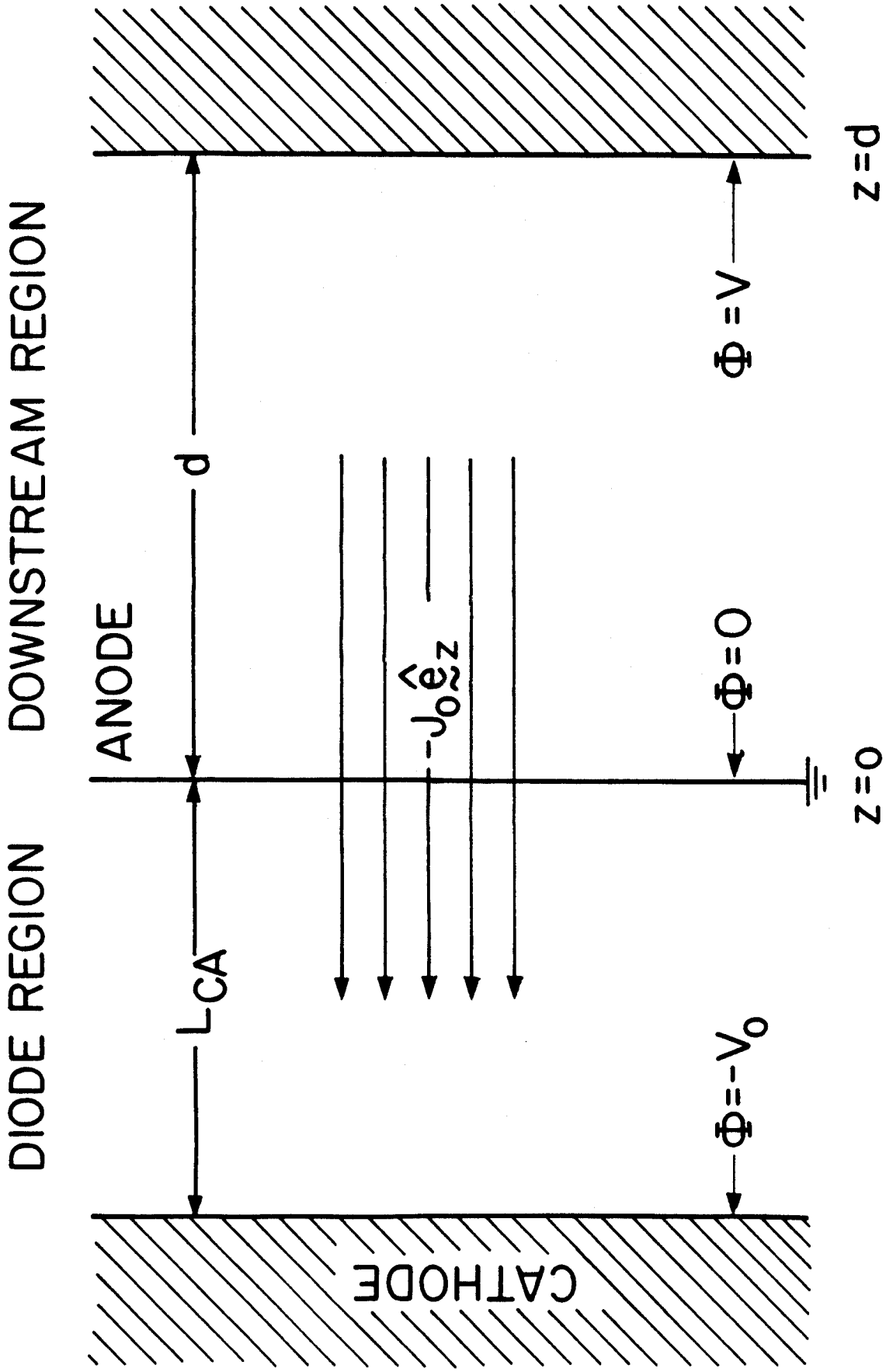
DIODE REGION
DOWNSTREAM REGION
CATHODE
ANODE
L_{CA}
d
$-J_o\hat{e}_z$
$\Phi=-V_o$
$\Phi=0$
$\Phi=V$
z=0
z=d

Fig. 1

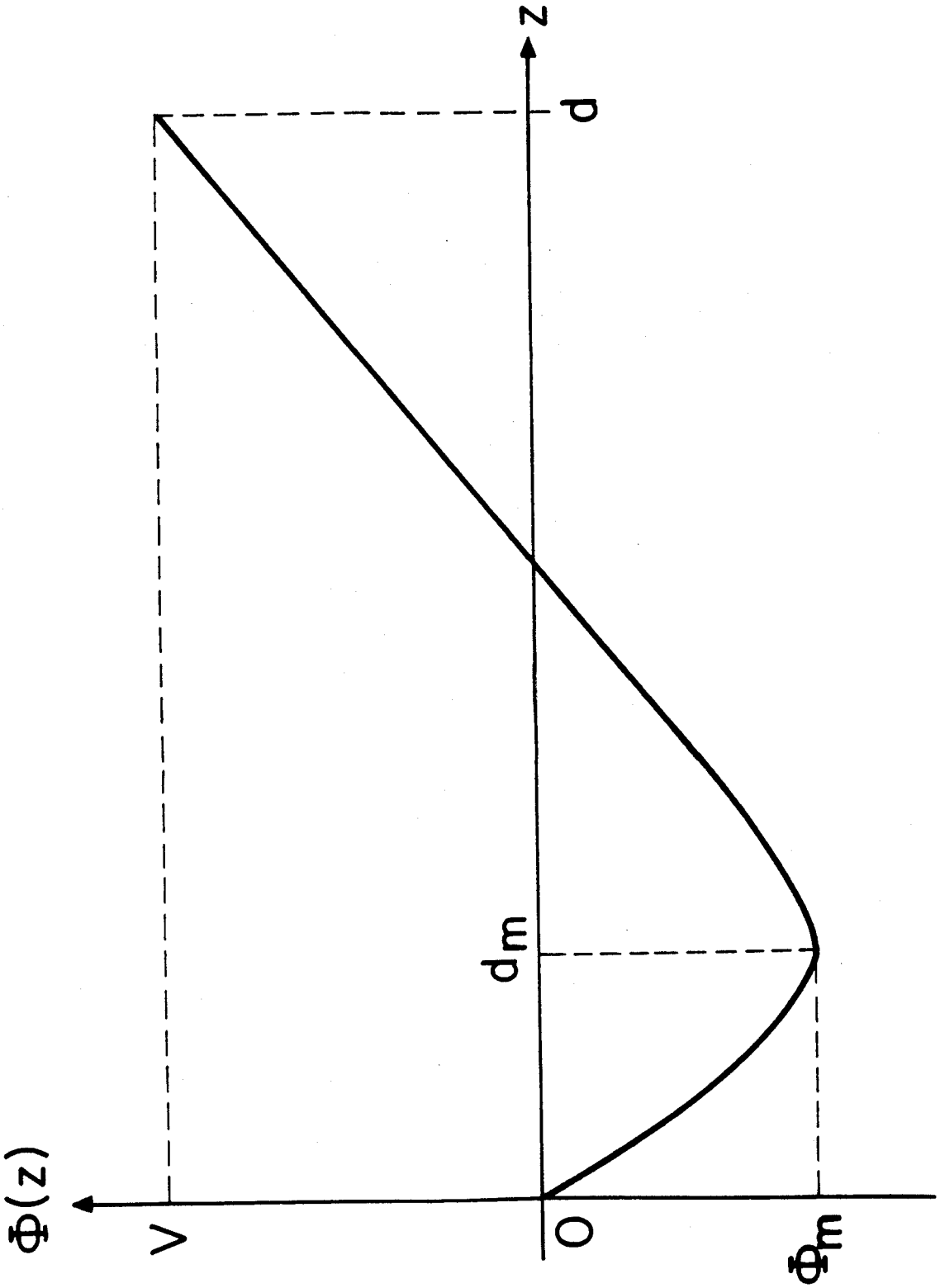

Fig. 2

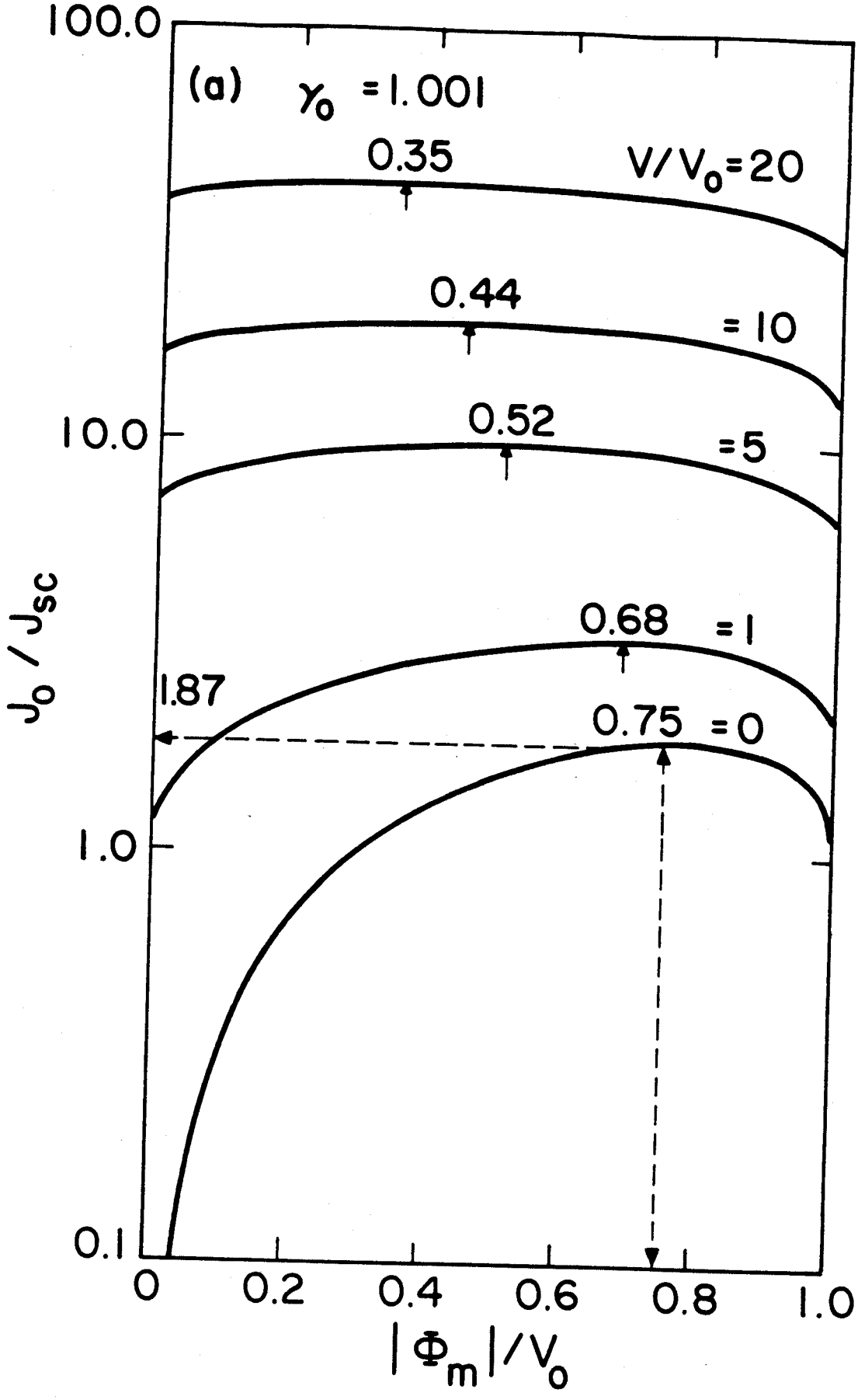
100.0
(a) γ_0 = 1.001
0.35
V/V_0=20
0.44
=10
10.0
0.52
=5
J_0 / J_{sc}
0.68
=1
1.87
0.75
=0
1.0
0.1
0
0.2
0.4
0.6
0.8
1.0
$|\Phi_m|/V_0$

Fig. 3(a)

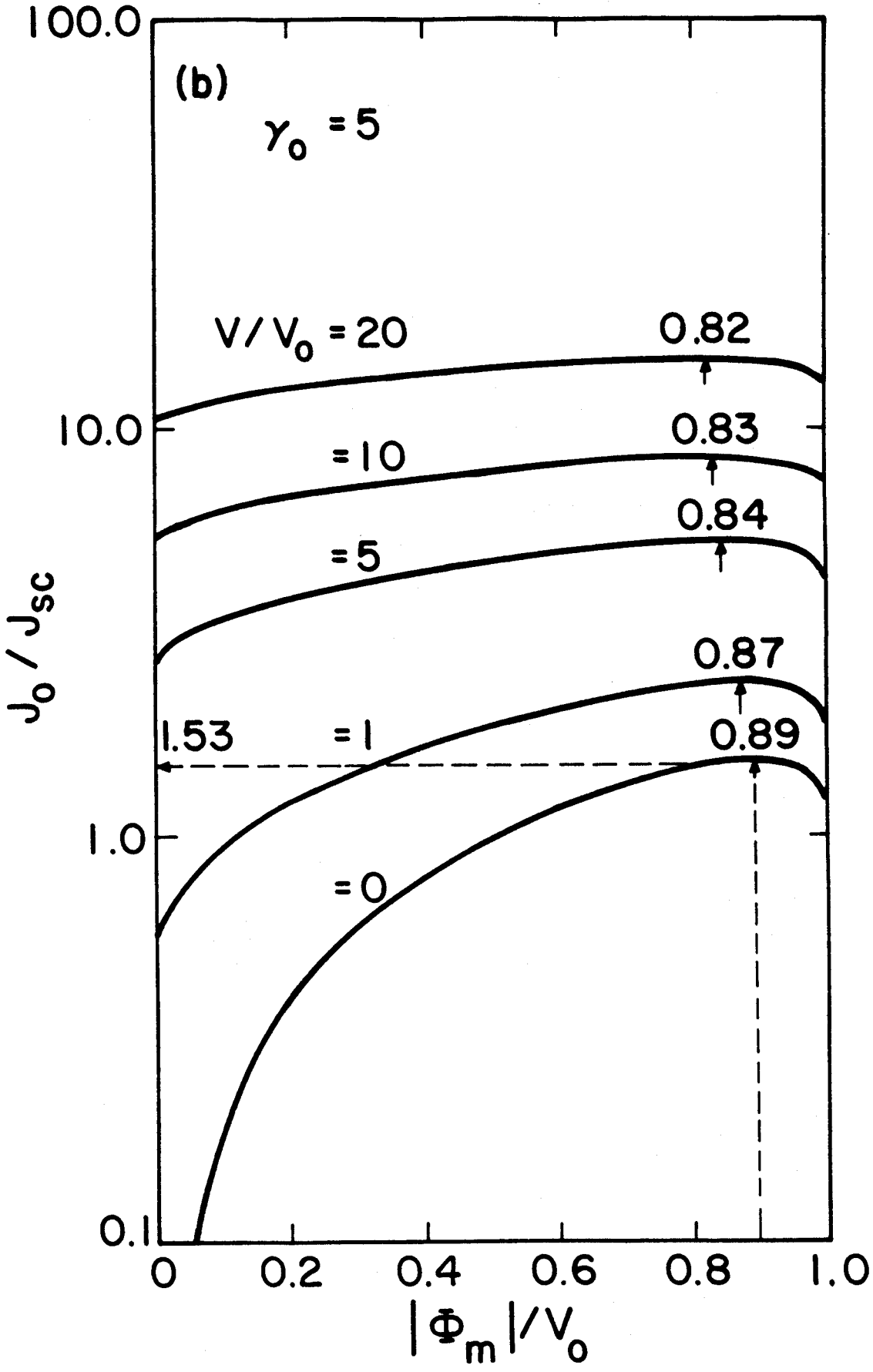
100.0
(b)
$\gamma_0 = 5$
$V/V_0 = 20$
0.82
10.0
=10
0.83
0.84
=5
0.87
1.53
=1
0.89
1.0
=0
0.1
J_0 / J_{sc}
0
0.2
0.4
0.6
0.8
1.0
$|\Phi_m|/V_0$

Fig. 3(b)

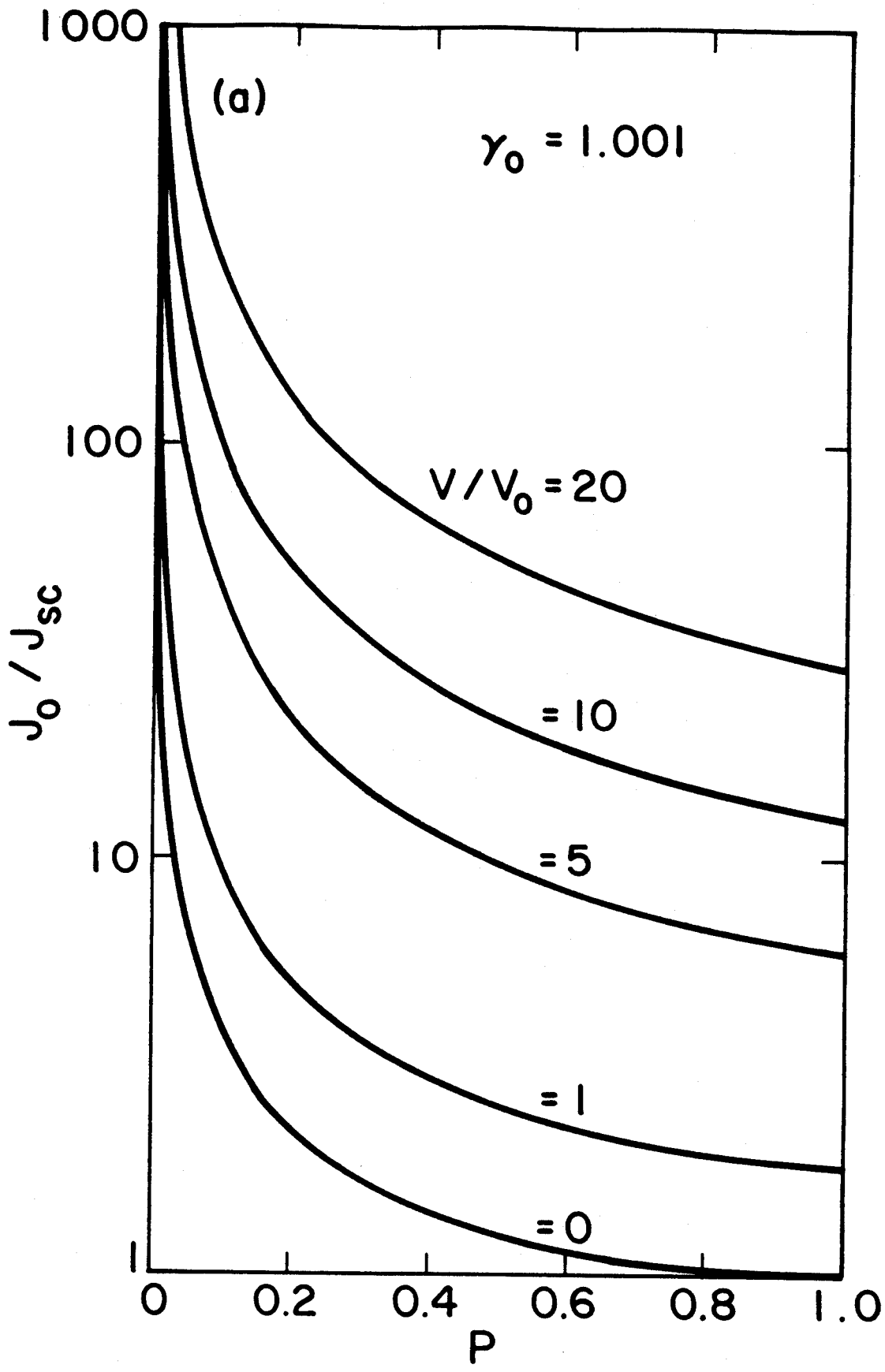

Fig. 4(a)

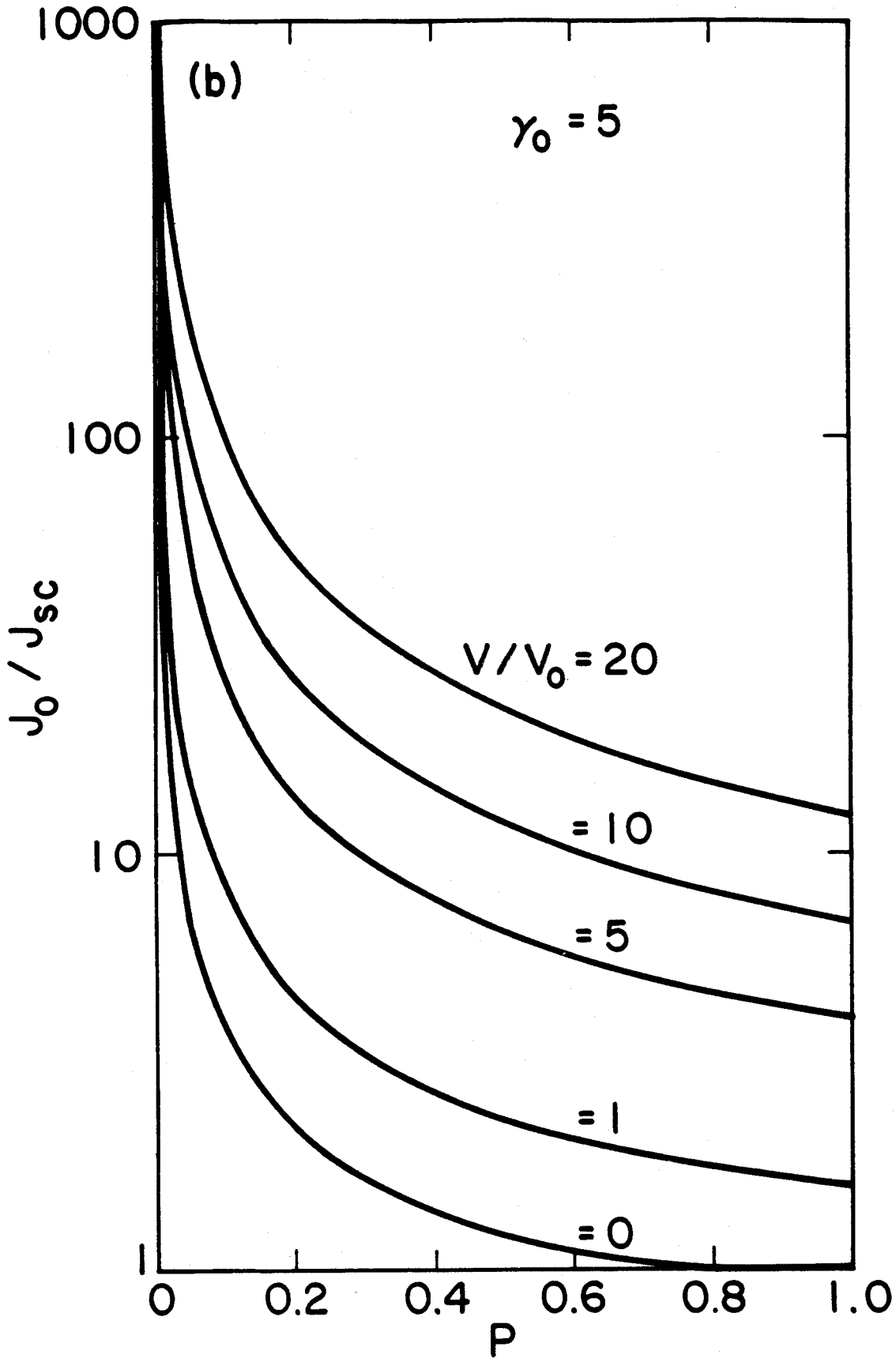

Fig. 4(b)

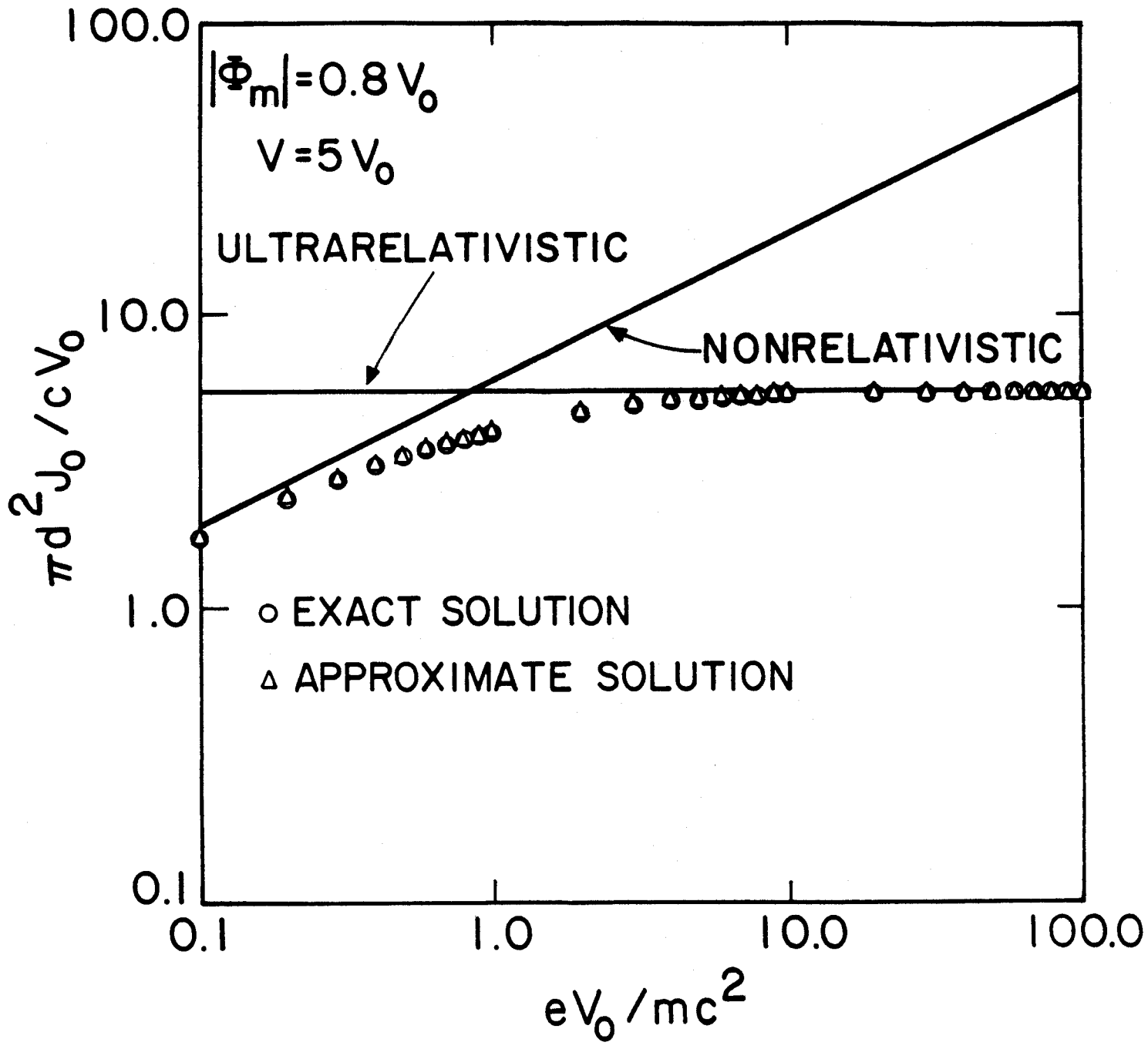
100.0
10.0
1.0
0.1
0.1
1.0
10.0
100.0
$|\Phi_m| = 0.8\,V_0$
$V = 5\,V_0$
ULTRARELATIVISTIC
NONRELATIVISTIC
o EXACT SOLUTION
Δ APPROXIMATE SOLUTION
$\pi d^2 J_0 / c V_0$
eV_0 / mc^2

Fig. 5

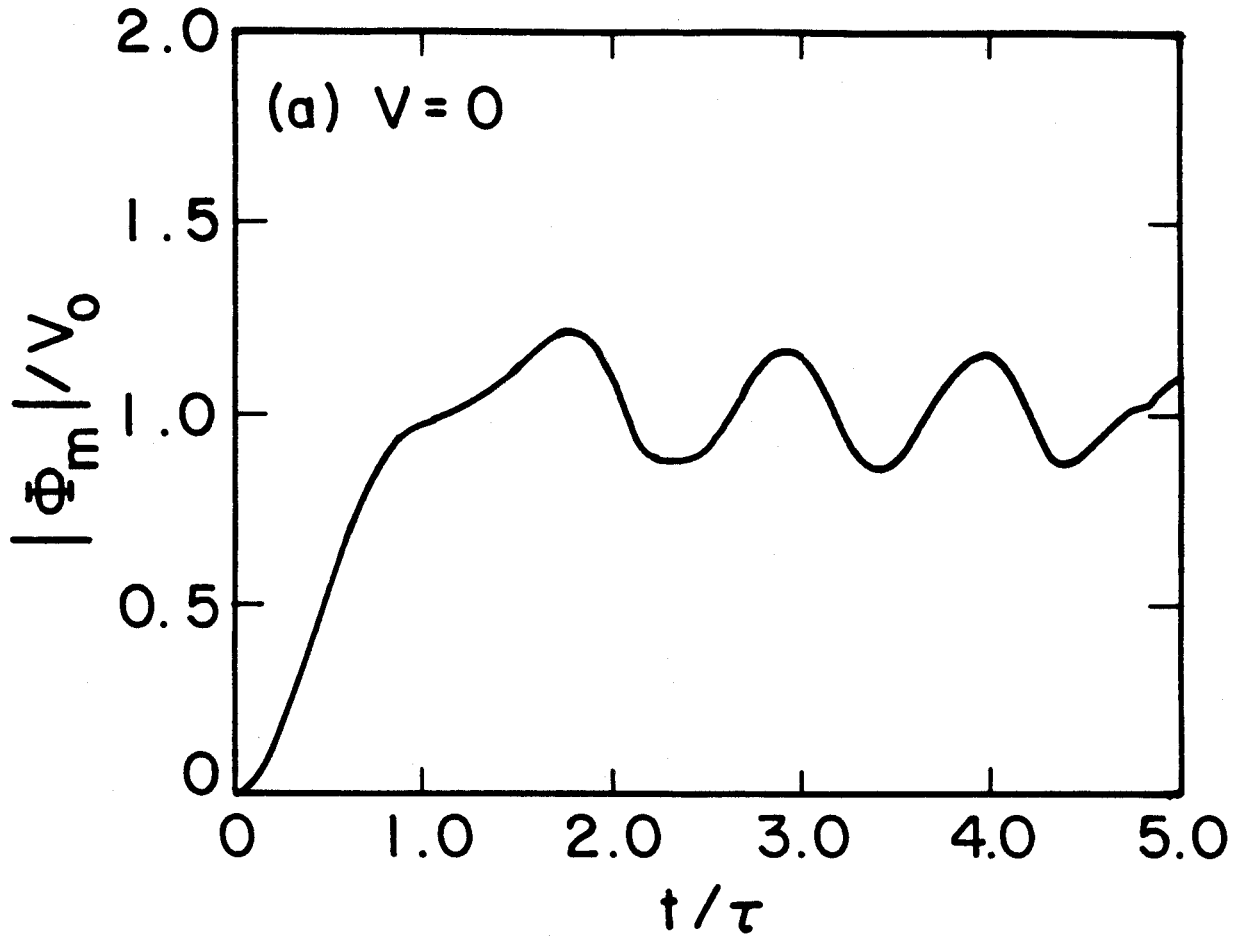

Fig. 6(a)

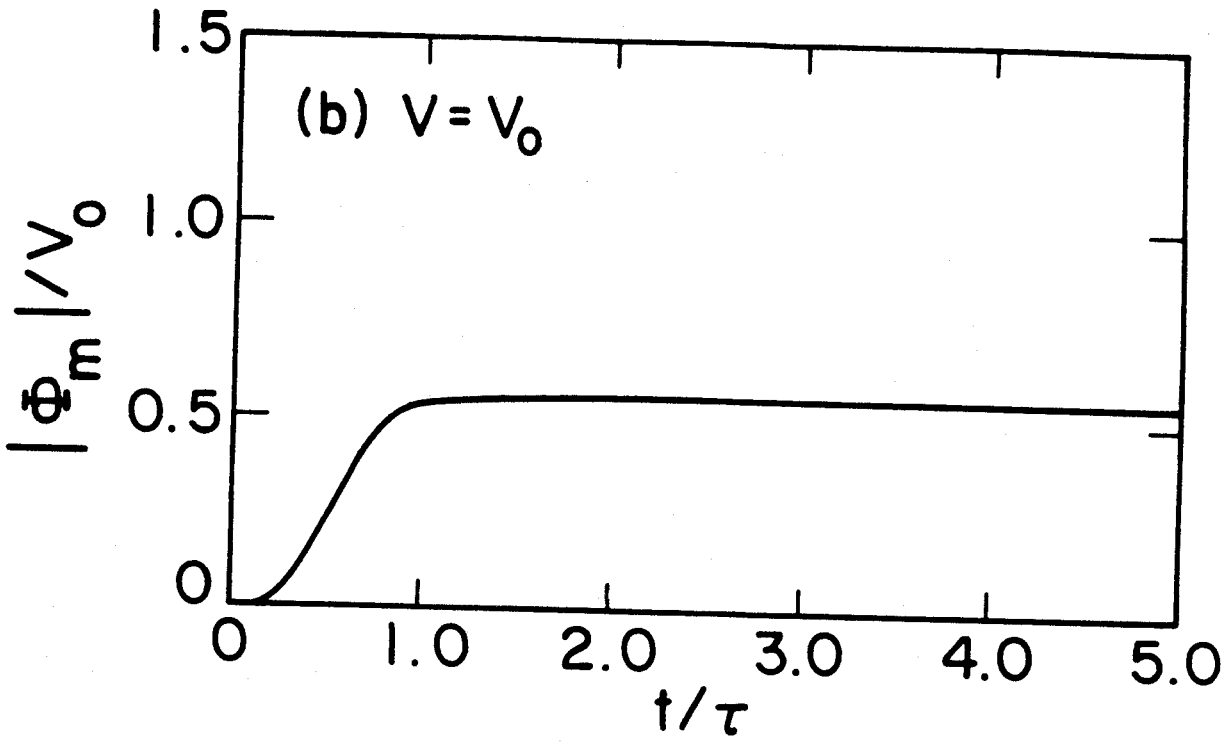

Fig. 6(b)

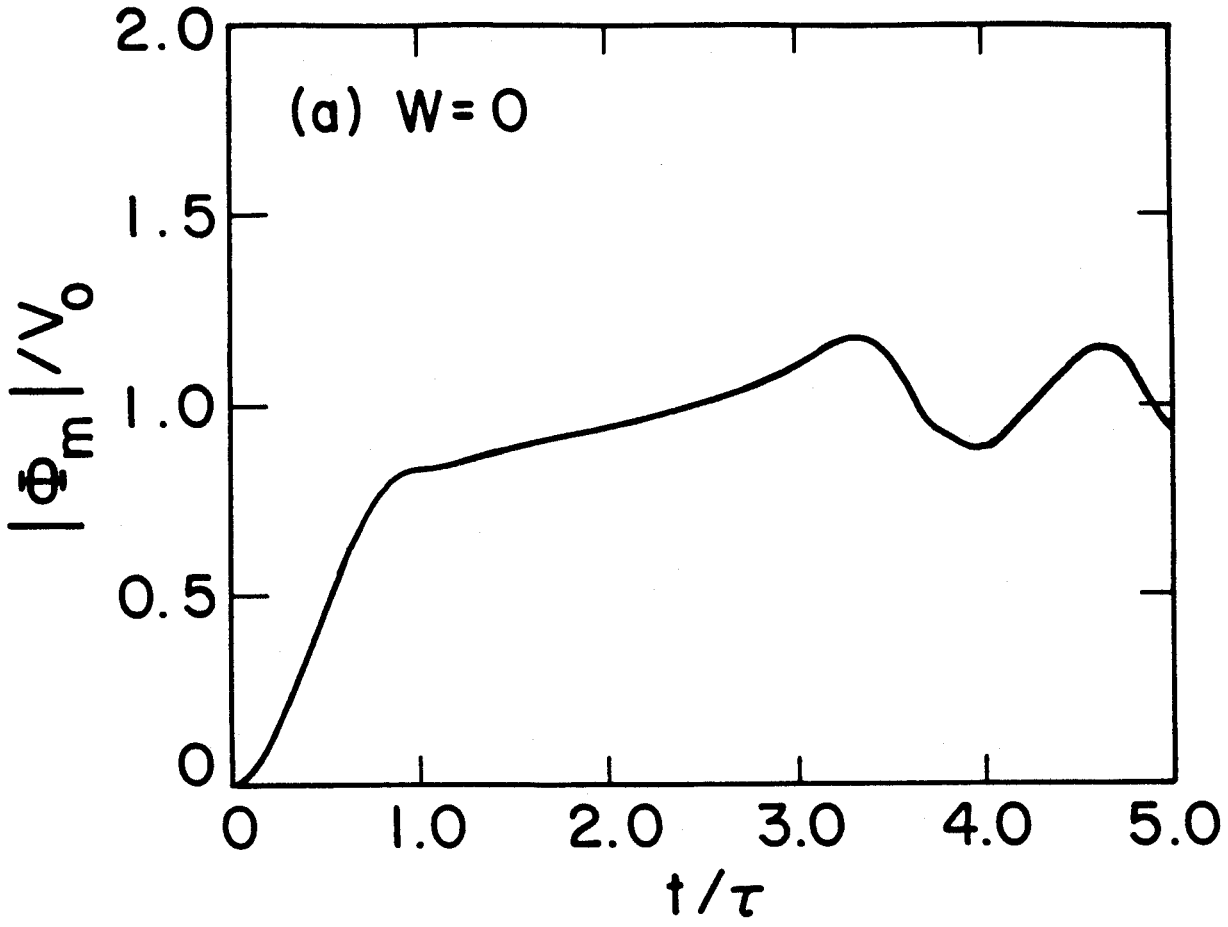

Fig. 7(a)

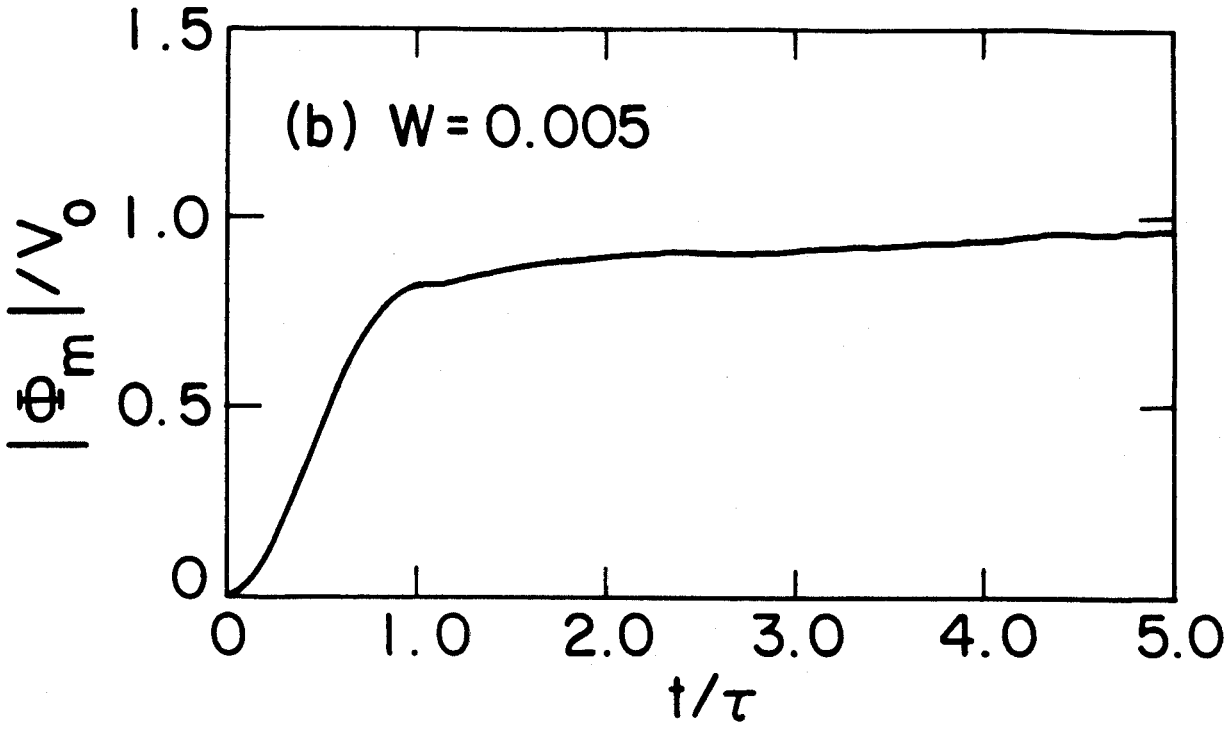

Fig. 7(b)

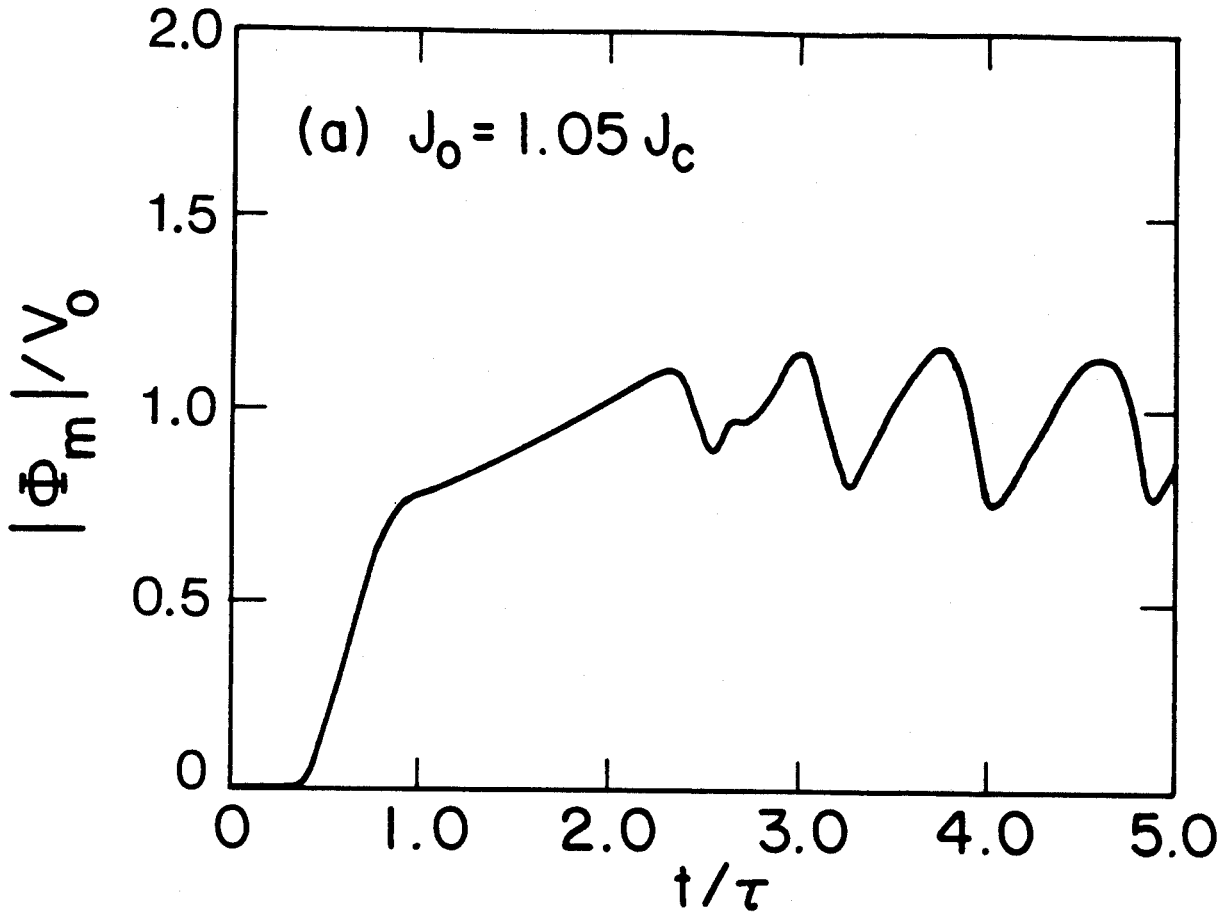

Fig. 8(a)

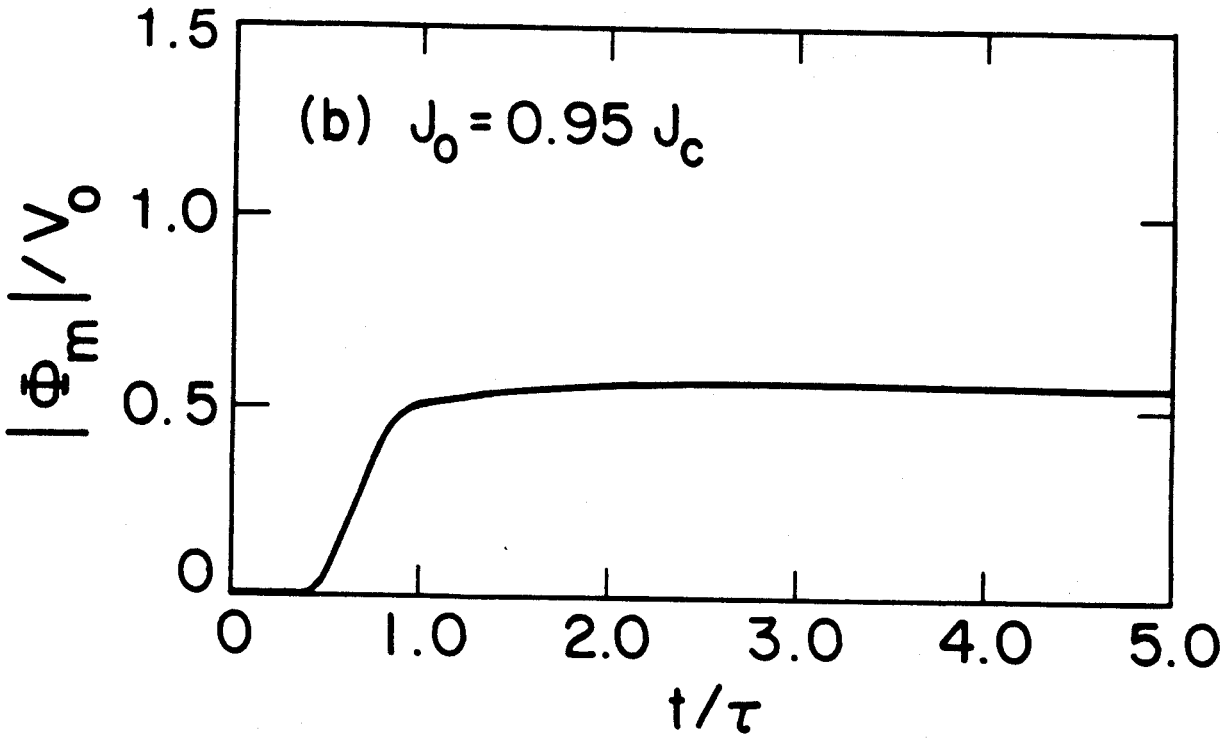

Fig. 8(b)